A model of stable functioning of the single branch pulsating heat pipe

Vadim S Nikolayev, Fabrice N Fourcade

A model of stable functioning of the single branch pulsating heat pipe

Vadim S. Nikolayev and Fabrice N. Fourcade
Université Paris-Saclay, CEA, CNRS, SPEC, 91191 Gif-sur-Yvette Cedex, France

E-mail: vadim.nikolayev@cea.fr

Abstract. A simplified model nonlinear describing the stable functioning of the single branch PHP is proposed. It is based on the earlier proposed film evaporation-condensation approach and assumes harmonic oscillations of the meniscus displacement and vapor pressure. The model predicts the frequency as a function of the oscillation amplitude and the relationship between the amplitudes of meniscus displacement and pressure. Results of the model are compared to available in the literature experimental data of different groups; they show a good agreement. The added mass caused by the oscillating flow in the liquid plug is discussed.

1. Introduction

The pulsating (or oscillating) heat pipe (PHP) is a capillary tube that meanders between hot and cold spots that form evaporator and condenser sections, respectively. The tube is filled with a pure fluid in such a way that liquid plugs and gas bubbles coexist inside. When the temperature difference between the evaporator and condenser exceeds a threshold, the self-sustained oscillations of the plugs and bubbles appear. The PHP is extremely attractive for various industrial applications because of high thermal performance and manufacturing simplicity. However the PHP functioning is not completely understood. The absence of predictive tools for its dimensioning is a substantial obstacle to its practical application. The reason for that is, on one hand, a multitude of complex physical phenomena involved into the PHP functioning [1], and on the other, its intrinsic non-stationarity.

Finding conditions of stable functioning of a PHP is one of the most important issues that is far from being solved. It is widely discussed in the literature. In the multi-branch PHP, the oscillations are chaotic in most cases. However, in some cases, a dominant oscillation frequency can be distinguished. It is characteristic of the small-amplitude oscillation regime where the oscillations are close to harmonic. They can be observed for a long time in a micro-PHP where the viscous losses are high [2] or intermittently [3]. The simulations show [4] that small-amplitude oscillations indeed occur in the intermittent oscillation regime, during the oscillation restart after a stopover. There are many oscillation modes in the multi-branch PHP, so the oscillations are not easy to understand theoretically, and empirical model components are necessary [2]. In this article we consider the simplest, single branch PHP, which is a capillary sealed from the
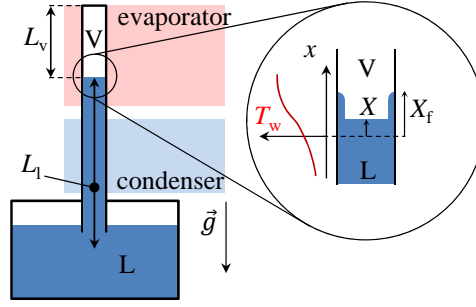
Figure 1. General scheme of the single branch PHP in the vertical position and a zoomed tube portion around the average meniscus position at small-amplitude oscillations; the local wall temperature variation is shown. L and V denote the liquid and vapor phases.

evaporator end and open at the condenser end, so the pressure is constant there (Fig. 1). The modeling remains however complex even in this simplest case because of the thermal interaction of the PHP tube with a thermal gradient along it [5], and the fluid motion, which makes the problem nonlinear. It would be desirable to have the relationships as simple as possible to describe the stable PHP oscillation regime. This is our objective.

The order of value of frequency of oscillations in the single branch PHP is given by its natural frequency (i.e. that calculated in the adiabatic case neglecting the energy dissipation) of the liquid column [6] of the average length $\bar{L}_{\text{l}}$. During oscillations, it adiabatically compresses the vapor bubble of the average length $\bar{L}_{\text{v}}$. For a vertical tube,

$$\omega_0 = \sqrt{\frac{\gamma \bar{p}}{\rho_{\text{l}} \bar{L}_{\text{l}} \bar{L}_{\text{v}}} + \frac{g}{\bar{L}_{\text{l}}}}, \tag{1}$$

where overbars mean time average. Since the single-branch PHP is often open to a reservoir (Fig. 1), L_{l} includes a contribution (the effective length of added mass) from the liquid oscillating in the reservoir. Note that $\bar{p}$ is the reservoir pressure corrected for the hydrostatic contribution corresponding to the average liquid column height.

2. Heat and mass exchange model

The model below is a simplification of the film evaporation-condensation model developed earlier [5, 6]. The system is assumed to be slightly above the oscillation start-up threshold. As a consequence, the heat and mass exchange is not too strong and the oscillations are close to harmonic; $X = A\cos(\omega t)$ is the displacement of meniscus from the neutral position $x = 0$, cf. Fig. 1. This means that while the amplitude of oscillations is not necessarily small, the system can be considered in the linear approximation as if the deviations (denoted with δ) around the time-averaged positions (denoted with overbars) were small.

The second simplification is introduced next. As the mass exchange is weak, its impact on the film length is neglected: the film edge is assumed to remain pinned at the position of the largest meniscus displacement $x = A$ so the film extends from $x = X$ to $x = X_{\text{f}} = A$. This assumption is justified by a weak contact line receding observed experimentally [7–9].

The heat flux through the liquid film

$$q_{\text{l}}(x) = k_{\text{l}} \frac{T_{\text{w}}(x) - T_{\text{sat}}}{h_{\text{l}}}, \tag{2}$$

where T_{w} is the temperature of the internal tube wall. Since the vapor-side heat flux at the liquid-vapor interface can be neglected with respect to the liquid-side heat flux q_{l}, the energy

conservation at the film interface implies that the mass evaporation rate is

$$\dot{m} = \frac{2\pi}{\mathcal{L}} \int_X^A (r - h_l) q_l(x) \mathrm{d}x \simeq \alpha(\Delta T + \delta T_{\text{sat}})(X - A), \tag{3}$$

where dot denotes the time derivative, $\alpha = 2\pi k_l(r - \bar{h}_l)/(\bar{h}_l \mathcal{L})$, and $\Delta T = \bar{T}_{\text{sat}} - \bar{T}_{\text{w}}$ is the tube wall subcooling at the neutral point of oscillation $x = 0$, $\bar{T}_{\text{w}} = T_{\text{w}}(x = 0)$. Note that the neutral point can be different from the meniscus position at equilibrium (where ΔT is necessarily zero [5]). During development of the self-sustained oscillations, the neutral (i.e. the moving average) position can shift in time to a new stable value, see e. g. Fig. 2 of [10]. For this reason, ΔT can be of either sign.

Because of linearization, only a time- and space-averaged film thickness $\bar{h}_l$ enters the above expressions. It can be assumed to be defined by the RMS velocity with the Aussillous and Quéré formula [11]. As justified by numerous experimental observations [7, 8], thin liquid films are deposited by the receding liquid menisci during their oscillation inside the PHP tube [12]. Because of their small thermal resistance, it is the main channel for the heat and mass exchange that drives the self-sustained oscillations. As only an averaged film thickness matters, the model is invariant of the specific film shape models discussed by Bae *et al.* [13].

Another important component of the model is the vapor energy balance [14]

$$m c_v \dot{T} = -p\dot{V} + RT\dot{m} + Q, \tag{4}$$

where T is the temperature of the vapor bulk. A boundary layer is formed in the vicinity of the vapor borders, in particular with the liquid at T_{sat} and with the dry wall that is assumed to be at the evaporator temperature T_{e}. The sensible heat received by the vapor from the dry portion of the tube is

$$Q = \text{Nu}\, k_v \pi \int_{X_f}^{\bar{L}_v} (T_{\text{w}}(x) - T) \mathrm{d}x \simeq \text{Nu}\, k_v \pi L_d (T_{\text{e}} - T), \tag{5}$$

where $\text{Nu} \simeq 6$ [15] at oscillations, $L_d = \bar{L}_v - A$ is the dry portion length, and T_{e} is the average evaporator temperature. Similarly to the previous works, the heat received from the wet portion can be neglected thanks to the smallness of the difference $(T - T_{\text{sat}})$. From Eqs. (4,5), one readily obtains that $\bar{T} = T_{\text{e}}$ and

$$\bar{m} c_v \delta \dot{T} = S\bar{p}\dot{X} + R\bar{T}\delta \dot{m} - \text{Nu}k\pi L_d \delta T, \tag{6a}$$

where the equality $\delta V = -SX$ (cf. Fig. 1) is used. By further linearizing Eq. (3) one gets

$$\delta \dot{m} = \alpha \left(X\Delta T - A \left. \frac{\mathrm{d}T_{\text{sat}}}{\mathrm{d}p} \right|_{\bar{p}} \delta p \right). \tag{6b}$$

Although this expression is harmonic in time, there is a term quadratic in A (because $\delta p \sim A$), which makes this system nonlinear. Note that the film evaporation term is at the origin of this nonlinearity, just like the nonlinear term in the previous model [5].

To close the model, one needs to express δp by varying the ideal gas law $p = mRT/V$ that describes the vapor behavior:

$$\delta p = \frac{\bar{p}}{\bar{m}}\delta m + \bar{\rho}R\delta T + \frac{\bar{p}}{\bar{V}}SX. \tag{6c}$$

The variables δp, δm, δT, and X are made dimensionless with the characteristic scales $\bar{p}SA/\bar{V}$, $\bar{\rho}SA$, $\bar{T}SA/\bar{V}$, and A, respectively. It is convenient now to introduce the dimensionless

constants

$$N_A = A\alpha \left.\frac{dT_{\text{sat}}}{dp}\right|_{\bar{p}} \frac{R\bar{T}}{\bar{V}\omega_0}, \tag{7a}$$

$$N_{\text{r}} = \frac{\alpha\Delta T}{\bar{\rho}S\omega_0}, \tag{7b}$$

$$N_{\text{d}} = \text{Nu}\frac{k_{\text{v}}\pi L_{\text{d}}}{\bar{m}c_v\omega_0}; \tag{7c}$$

and the dimensionless frequency $\hat{\omega} = \omega/\omega_0$, where ω_0 is given by one of Eqs. (1) depending on the PHP orientation. Note that N_A and N_{d} are both positive while N_{r} can be of either sign.

Next, the Fourier transform can be applied to Eqs. (6). They become

$$i\hat{\omega}\tilde{T} = (\gamma - 1)i\hat{\omega}(\tilde{X} + \tilde{m}) - N_{\text{d}}\tilde{T}, \tag{8a}$$

$$i\hat{\omega}\tilde{m} = N_{\text{r}}\tilde{X} - N_A\tilde{p}, \tag{8b}$$

$$\tilde{p} = \tilde{m} + \tilde{X} + \tilde{T}, \tag{8c}$$

where i is the imaginary unit, the tilde corresponds to the Fourier counterparts of the dimensionless quantities introduced earlier, and γ is the adiabatic index. We can now find the relation between the pressure and the displacement:

$$\tilde{p} = \frac{-\hat{\omega}^2\gamma + i(\gamma N_{\text{r}} + N_{\text{d}})\hat{\omega} + N_{\text{r}}N_{\text{d}}}{-\hat{\omega}^2 + i(N_{\text{d}} + \gamma N_A)\hat{\omega} + N_{\text{d}}N_A}\tilde{X}. \tag{9}$$

3. Frequency analysis

The last governing equation has not been used up to now. It is the momentum balance of a liquid plug of the mass $m_{\text{l}} = \rho_{\text{l}}L_{\text{l}}S$. It can be obtained by averaging the Navier-Stokes equation (20) over the tube cross-section,

$$m_{\text{l}}\ddot{X} = -S\delta p - F, \tag{10}$$

where F is the viscous friction force (see Appendix). In the dimensionless Fourier representation,

$$-\hat{\omega}^2\tilde{X} = -\frac{\tilde{p}}{\gamma} - 2i\hat{\omega}\frac{G}{\text{Re}_{\omega 0}}\tilde{X}, \tag{11}$$

where the function $G = G(\hat{\omega}\text{Re}_{\omega 0})$ is given by Eq. (22) and $\text{Re}_{\omega 0} = \omega_0 r^2/\nu$. We are interested in the established oscillation regime so $\hat{\omega}$ is real. The substitution of Eq. (9) results in two equalities, those of real and imaginary parts. The equality of the real parts defines the oscillation frequency:

$$\gamma\hat{\omega}^2\left\{1 + \frac{2Im[G(\hat{\omega}\text{Re}_{\omega 0})]}{\hat{\omega}\text{Re}_{\omega 0}}\right\} = \frac{\gamma\hat{\omega}^4 + \left[N_{\text{d}}^2 + (\gamma - 1)N_{\text{r}}N_{\text{d}} + N_{\text{r}}N_A\gamma^2\right]\hat{\omega}^2 + N_{\text{r}}N_A N_{\text{d}}^2}{\hat{\omega}^4 + \left[N_{\text{d}}^2 + 2(\gamma - 1)N_A N_{\text{d}} + \gamma^2 N_A^2\right]\hat{\omega}^2 + N_A^2 N_{\text{d}}^2}. \tag{12}$$

The equality of the imaginary parts of Eq. (11) means that the energy brought via phase change is equal to the dissipation so this condition results in an expression that fixes the amplitude A of oscillations. This important parameter is however difficult to evaluate theoretically. Apart from the energy dissipation related to the vapor heat exchange with the tube wall [10] and the viscous losses in the plug accounted in the present model, the amplitude is limited by the viscous dissipation in the contact line vicinity (known to be important [16]) and the pressure losses related to the connection of PHP channel to a reservoir (Fig. 1) [8], which are not easy to evaluate with precision.
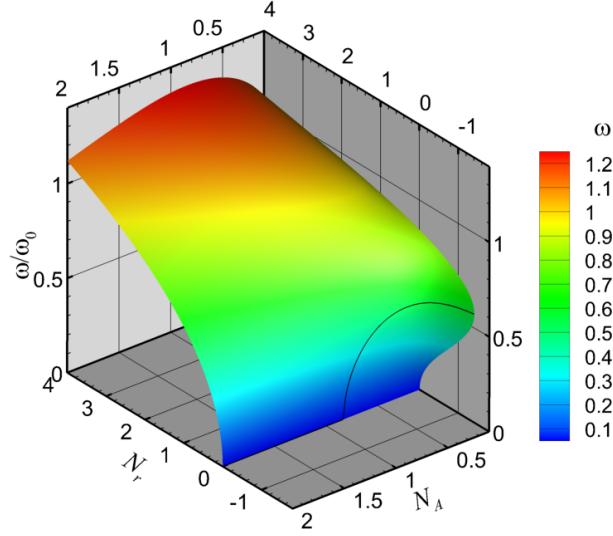
Figure 2. The frequency as a function of the parameters N_{r} and N_A calculated for $N_{\text{d}} = 1$ and $\text{Re}_{\omega 0} = 12$. The black line consists of points of minimum of the curve $N_{\text{r}}(\omega)$ (the minimum is calculated while N_A is kept fixed).

3.1. Frequency of self-sustained oscillations

Note that both left and right hand sides of Eq. (12) are even with respect to $\hat{\omega}$ so one can search the positive roots only. The frequency of the self-sustained oscillations can only be obtained by solving Eq. (12) numerically. The numerical calculation is shown in Fig. 2, where $\hat{\omega}$ is given as a function of N_{r} and N_A. There are however two more parameters (N_{d} and $\text{Re}_{\omega 0}$) on which the frequency depends. They are both related to the energy dissipation. $\text{Re}_{\omega 0}$ corresponds to the viscous dissipation and enters the frequency expression through the factor (26). As shown in the Appendix, the amplitude of its variation is quite small ($\pm 5\%$) so it only weakly impacts the frequency. The factor N_{d} describes the heat exchange of the vapor with the environment, which creates an additional energy loss during oscillations [10]. As the frequency is generally only weakly dependent on the dissipation, the dependence on N_{r} and N_A remains at least qualitatively the same for all N_{d}, provided it is not too large to overdamp the oscillations.

Fig. 2 shows several general features. First, as usual for non-linear systems, the frequency depends on the oscillation amplitude (through the dimensionless parameter $N_A \sim A$). This dependence is non-monotonous. Generally, at small $N_A \lesssim 1$, ω grows with N_A, while at large $N_A \gtrsim 1$, a decrease is observed.

The dependence on N_{r} is non-trivial (recall that N_{r} can be of either sign). For N_A larger than a critical value $N_A^{\text{cr}} \simeq 0.82$ that is almost independent of N_{d} and $\text{Re}_{\omega 0}$, Eq. (12) has a unique root $\omega = \omega_1$ that grows with N_{r} and has a property $\omega_1(N_{\text{r}} \to 0) \to 0$ (Fig. 2), so the oscillations are possible only for a positive N_{r}. For $N_A < N_A^{\text{cr}}$, oscillations are possible also for negative N_{r} larger than a minimal value that grows with N_A and attains zero for $N_A = N_A^{\text{cr}}$. Two roots thus exist for $N_{\text{r}} < 0$, ω_1 and $\omega_2 \leq \omega_1$. The roots are equal at the minimal $N_{\text{r}} < 0$, which is thus the bifurcation point (Fig. 2). While ω_1 increases with N_{r}, ω_2 decreases to zero when $N_{\text{r}} \to 0$.

Although it is evident that the rigorous value for the frequency of the self-sustained oscillations can only be obtained by solving Eq. (12) numerically, one can discuss some asymptotic results applicable in the assumption that the added mass can be assumed constant (which is valid at very high or very low frequencies). First one mentions (cf. Fig. 4) that the factor (26) that appears because of the viscous dissipation, is bounded and varies only within 10%.

In the case where N_A, N_d, and N_r are small (small impact of mass exchange), one gets

$$\frac{\omega}{\omega_0 f(\omega_0)} = 1 + N_d \frac{1-\gamma}{2\gamma}(N_d - N_r) + N_A \left[N_r \frac{\gamma}{2} + N_d(1-\gamma) \right] - N_A^2 \frac{\gamma^2}{2}. \tag{13}$$

One can see clearly that the deviation of ω from ω_0 is provided by the viscous effect and the heat exchange. In the opposite case, where the phase change controls completely the frequency, N_A, N_d, and $N_r \gg 1$ and

$$\omega = \omega_0 f(\omega_0) \sqrt{\frac{N_r}{\gamma N_A}}. \tag{14}$$

These expressions show that depending on the relation between above three constants, the frequency can either grow or decrease with the oscillation amplitude A.

4. Physical meaning of the dimensionless numbers N_A and N_r
We show below that N_A and N_r can be expressed in terms of tree different contributions to the vapor mass change over the characteristic time $\sim \omega^{-1}$ of oscillation, during which the meniscus recedes by the length A: δm_{pconst}, δm_V, and δm_p explained next. The total vapor mass change is obtained by rewriting Eq. (6c) as

$$\frac{\delta m}{\bar{m}} = \frac{\delta p}{\bar{p}} + \frac{\delta V}{\bar{V}} - \frac{\delta T}{\bar{T}}. \tag{15}$$

The vapor mass change $\delta m_{pconst} = \bar{\rho}\delta V = \bar{\rho}SA$ is given by the second term in Eq. (15) and corresponds to the vapor mass necessary to provide the isobaric meniscus receding. When the generated vapor mass is larger than δm_{pconst}, the pressure grows when meniscus recedes so the meniscus rebound (and thus oscillation) becomes difficult unless the pressure drops because of another reason.

δm_V is the vapor mass change due to the evaporation from the film formed during the meniscus receding. According to Eq. (3),

$$\delta m_V \sim \dot{m}/\omega \sim \frac{2\pi(r - \bar{h}_l)}{\mathcal{L}\omega} \frac{k_l \Delta T}{\bar{h}_l} A = \frac{\alpha \Delta T A}{\omega} \tag{16}$$

The ratio $\delta m_V / \delta m_{pconst}$ is thus a parameter characterizing the meniscus rebound: the rebound is small when $\delta m_V > \delta m_{pconst}$ because the evaporation provides enough vapor to maintain the constant pressure. The rebound is important when $\delta m_V / \delta m_{pconst} < 1$. From the definition (7b), it is evident however that $\delta m_V / \delta m_{pconst} \sim N_r$.

The frequency is also impacted by the vapor mass change associated with the evaporation rate change caused by T_{sat} variation during oscillations, $\delta m_p \sim \dot{m}/\omega \sim \alpha \delta T_{sat} A/\omega$, where $\delta T_{sat} \sim \delta p \, dT_{sat}/dp$. The pressure change is mainly caused by the meniscus displacement with no change in T and m, $\delta p = -\bar{p}\delta V/\bar{V}$. Finally,

$$\delta m_p \sim -\alpha \left. \frac{dT_{\text{sat}}}{dp} \right|_{\bar{p}} \frac{\bar{p}A^2 S}{\omega \bar{V}} \tag{17}$$

The larger is $\delta m_p / \delta m_{pconst}$, the stronger is the vapor mass variation that causes the vapor pressure variation, which modifies the oscillation frequency ω_{nat} that system would have without mass exchange. The following relation holds

$$\frac{\delta m_p}{\delta m_{pconst}} \sim -N_A. \tag{18}$$

5. Comparison to the experimental data

One can hardly compare the oscillation frequency data with the experiment as the expressions (1) for ω_0 contain the parameter L_l that includes the effect of reservoir that cannot be predicted theoretically with certainty. In the only available in the literature experiment obtained without the reservoir [17], the amplitude of oscillation was so small (cf. Table 1 below) that $\omega \simeq \omega_0$ and the impact of different parameters is difficult to appreciate.

One can compare the amplitude P of pressure oscillations with the experimental data. The theoretical value can be obtained as an absolute value of the pressure variation (9). We present it below in the dimensional form:

$$P = \frac{\bar{p}AS}{\bar{V}} \sqrt{\frac{(\hat{N}_r^2 + 1)(\hat{N}_d^2 + \gamma^2)}{1 + \gamma^2 \hat{N}_A^2 + 2(\gamma - 1)\hat{N}_d \hat{N}_A + \hat{N}_d^2(1 + \hat{N}_A^2)}}, \qquad (19)$$

where the constants with the hats are related to the no-hat counterparts as $\hat{N}_i = N_i/\hat{\omega}$ so they include ω instead of ω_0, cf. Eqs. (7). A remarkable feature of Eq. (19), which is the central result of this article, is its independence of ω_0. It contains only the parameters measurable experimentally so one can perform a direct comparison.

In the linear regime, one expects $P \propto A$. According to Eq. (19), this is true only for small $\hat{N}_A$. For $\hat{N}_A \gg 1$, P becomes to be independent of A.

The phase shift between the pressure and displacement is more delicate to compare because of the difficulty to extract it from the existing experimental data where many harmonics are usually present.

The following procedure has been used for comparison with experiments. First, the experimental amplitudes of the pressure P_{exp} and the meniscus displacement A are identified. For some experiments, A needs to be estimated if the meniscus goes out of view field of camera. In all the considered data sets, the temperatures of evaporator T_e and condenser T_c were aimed to be imposed. However, as the capillaries are made of glass, which is a poor heat conductor, a smooth internal wall temperature variation actually ocurred. The internal wall temperature $T_c \leq \bar{T}_w \leq T_e$ is estimated from the position of neutral point $x = 0$. This position is also used to calculate $\bar{V}$ that also includes the dead vapor volume. The experimental average pressure $\bar{p}$ and oscillation frequency are both well known for each experiment. The NIST REFPROP database is used to obtain the system parameters for each fluid. Based on $\bar{p}$, the saturation state parameters like $\bar{T}_{\text{sat}}$, $\mathcal{L}$, the saturation curve slope, etc. are calculated; the Aussillous and Quéré [11] formula is used for $\bar{h}_l$ by using the average meniscus receding velocity $\omega A/\sqrt{2}$. The vapor parameters are calculated for $\bar{p}$ and $\bar{T} = T_e > T_{\text{sat}}$. All these parameters are necessary to determine the $\hat{N}_i$ constants. Then the theoretical P value is determined with Eq. (19).

All (to our knowledge) existing single branch PHP experiments with published data on both pressure and displacement could be used for the comparisons except [8], where the film did not cover all the channel perimeter (contrary to what model assumes) because it was rectangular. The data are compelled in Table 1. It evidences a good quantitative agreement between P_{exp} and P, which shows the validity of our model.

Table 1. The parameters calculated using available in the literature experimental data. Note that $r = 1$ mm for all the cases except [17], where $r = 1.1$ mm, so the S values are similar. Two last columns present a comparison of the experimental pressure oscillation amplitude and its theoretical value.

Fluid	Ref.	$\bar{p}$ kPa	T_{e} °C	T_{c} °C	$\bar{V}$ cm^3	$\bar{h}_{\text{l}}$ μm	ω s^{-1}	A cm	$\bar{T}_{\text{w}}$ °C	T_{sat} °C	$\hat{N}_{\text{r}}$	$\hat{N}_A$	$\hat{N}_{\text{d}}$	P_{exp} Pa	P Pa
FC72	[7]	46.7	46	16	3.5	48.5	4.4	5	33.8	36.1	2.07	1.01	1.20	3500	3501
FC72	[7]	46.7	46	28	4.1	61.8	7.3	4.56	38.5	36.1	-1.01	0.37	0.77	2105	2182
pentane	[18]	53.9	42	-16	3.5	29.3	4.5	8	11.6	18.9	21.67	5.41	3.00	5000	5033
pentane	[6]	90.6	45	10	3.3	57.0	22.4	5	38	32.8	-0.90	0.24	0.33	5500	5528
pentane	[6]	90.6	65	0	3.6	82.9	18.5	12	5.8	32.8	4.07	0.46	0.52	40000	39999
water	[17]	101.3	104	20	1.2	7.1	108.9	0.093	95.5	100	5.38	0.1	1.27	1220	1230

Nomenclature

A meniscus oscillation amplitude [m]
c_v vapor specific heat at constant volume [J/(kg·K)]
F viscous friction force [N]
f viscous dissipation factor given by Eq. (26)
g gravity acceleration [m/s^2]
h_{l} liquid film thickness [m]
i imaginary unit
I_n modified Bessel function of the order n
Im imaginary part of a complex number
k vapor heat conductivity [W/(m·K)]
L length [m]
$\mathcal{L}$ latent heat [J/kg]
m vapor mass [kg]
N dimensionless number
Nu Nusselt number
P pressure amplitude [Pa]
p vapor pressure [Pa]
Q heat power [W]
q heat flux [W/m^2]
R gas constant for the vapor [J/(kg·K)]
Re$_\omega$ kinetic Reynolds number
r internal tube radius [m]

S capillary cross-section area [m^2]
T temperature [K]
t time [s]
u fluid velocity [m/s]
V vapor volume [m^3]
X meniscus displacement [m]
x axial coordinate [m]

Greek symbols
γ vapor adiabatic index
μ liquid shear viscosity [Pa·s]
ν liquid kinematic viscosity [m^2/s]
ω angular frequency [s^{-1}]
ρ vapor density [kg/m^3]
ϱ radial coordinate [m]

Subscripts
c condenser
e evaporator
exp experimental
f film edge (contact line)
l liquid
sat saturation
v vapor
w internal tube wall

Appendix: Laminar oscillating flow

The laminar flow can be induced in a capillary filled with a liquid by the periodic variation of the pressure gradient [19]. In our case, the periodic variation is caused by the heat and mass exchange. For a tube of the circular cross-section, this problem can be solved with the Fourier transform of the Navier-Stokes equation for the axial velocity component $u_x = u_x(\varrho, t)$,

$$i\omega\rho_{\text{l}}\tilde{u}_x = -\frac{\partial \tilde{p}_{\text{l}}}{\partial x} + \mu\nabla^2\tilde{u}_x, \qquad (20)$$

where hat means the Fourier transform of the dimensional variables, and $\varrho \in (0, r)$ is the radial coordinate. The no-slip boundary condition at $\varrho = r$ and finiteness of $\tilde{u}_x(0)$ result in the
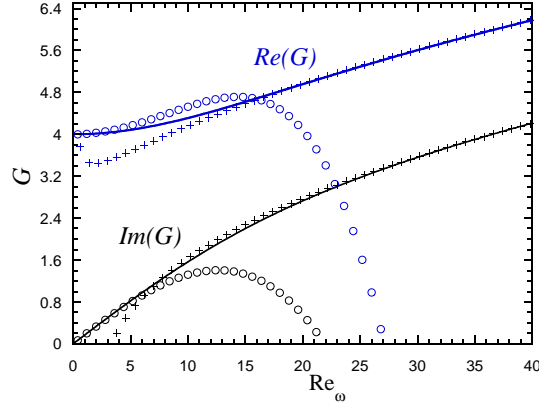
Figure 3. The real and imaginary parts of the function $G(\omega)$ (lines) and its approximations, for small (Eq. (23), circles) and large (Eq. (25), crosses) kinetic Reynolds numbers.

following expression [19]

$$\tilde{u}_x = \frac{1}{i\omega\rho_l}\frac{\partial \tilde{p}_l}{\partial x}\left(\frac{I_0(\chi\varrho)}{I_0(\chi r)} - 1\right). \tag{21}$$

where I_n is the modified Bessel function of the order n and $\chi = \sqrt{i\omega/\nu}$. This classical results can be easily exploited for our purpose as follows. The pressure gradient can be expressed through the averaged over tube cross-section liquid velocity $\upsilon = \dot{X}$. The force F exercised by the tube walls on the fluid is the shear stress integrated over the wall area; its Fourier transform is [16]

$$\tilde{F} = -2\pi r\mu L_l\left.\frac{\partial \tilde{u}_x}{\partial \varrho}\right|_{\varrho=r} = 2\pi\mu L_l\tilde{\upsilon}G(\omega), \quad G(\omega) = z\left(\frac{I_0(z)}{I_1(z)} - \frac{2}{z}\right)^{-1}, \tag{22}$$

which is a complex function of the kinetic Reynolds number $\text{Re}_\omega = \omega r^2/\nu$; $z = \chi r = \sqrt{i\text{Re}_\omega}$. One can show that the real part of G is an even function of Re_ω, while the imaginary part is an odd function. The real and imaginary parts of $G(\text{Re}_\omega)$ can be calculated with Wolfram Mathematica software. They are shown in Fig. 3 together with the asymptotic formulas discussed next. The expression (22) can be developed as a power series,

$$G(\omega) = 4 + \frac{i\text{Re}_\omega}{6} + \frac{\text{Re}_\omega^2}{144} - \frac{i\text{Re}_\omega^3}{2880} - \frac{7\text{Re}_\omega^4}{414720} + \mathcal{O}(\text{Re}_\omega^5), \tag{23}$$

valid for small frequencies. By performing the inverse Fourier transform, one gets from the first two terms

$$F = 8\pi\mu L_l\dot{X} + \frac{1}{3}m_l\ddot{X} \tag{24}$$

The first term is the Hagen-Poiseuille expression, and the second presents the first-order oscillation correction. Its particularity is that it is independent of viscosity and corresponds to the added mass of $m_l/3$.

For large Re_ω, the following approximation holds:

$$G(\omega) = \frac{(1+i)\sqrt{\text{Re}_\omega}}{\sqrt{2}} + \frac{3}{2} + \frac{15}{8}\left(\frac{1-i}{\sqrt{2\text{Re}_\omega}} - \frac{i}{\text{Re}_\omega}\right) + \mathcal{O}(\text{Re}_\omega^{-3/2}). \tag{25}$$

For the frequency calculation in sec. 3.1, the viscous dissipation factor

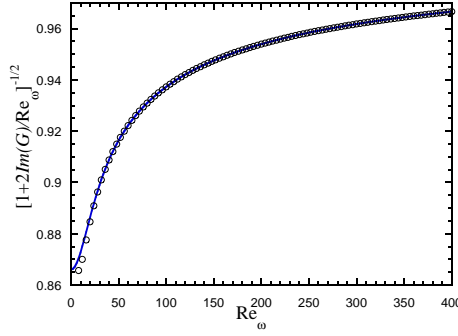$$f(\omega) = \left[1 + \frac{2Im(G)}{\text{Re}_\omega}\right]^{-1/2} \tag{26}$$

Figure 4. Viscous dissipation factor, Eq. (26) (line) and its approximation (27) (circles).

that enters Eq. (12) is important. Its dependence on ω is shown in Fig. 4. One can use the approximation (25) at large Re_ω that appears to be quite good,

$$f(\omega) = 1 - \frac{1}{\sqrt{2}}\mathrm{Re}_\omega^{-1/2} + \frac{3}{4\mathrm{Re}_\omega} + \frac{5}{8\sqrt{2}}\mathrm{Re}_\omega^{-3/2} + \frac{5}{32}\mathrm{Re}_\omega^{-2} + \mathcal{O}(\mathrm{Re}_\omega^{-5/2}). \tag{27}$$

References
[1] Nikolayev VS 2021 *Appl. Therm. Eng.* **195** 117111
[2] Yoon A and Kim SJ 2019 *Energy Convers. Manage.* **181** 48
[3] Perna R, Abela M, Mameli M, Mariotti A, Pietrasanta L, Marengo M and Filippeschi S 2020 *Appl. Therm. Eng.* **171** 115128
[4] Nekrashevych I and Nikolayev VS 2019 *Microgravity Sci. Technol.* **31** 241 . Issue on Heat pipe systems for thermal management in space
[5] Nikolayev VS 2016 *Int. J. Heat Mass Transfer* **95** 477
[6] Das SP, Nikolayev VS, Lefèvre F, Pottier B, Khandekar S and Bonjour J 2010 *Int. J. Heat Mass Transfer* **53** 3905
[7] Rao M, Lefèvre F, Khandekar S and Bonjour J 2015 *Int. J. Heat Mass Transfer* **86** 519
[8] Fourgeaud L, Nikolayev VS, Ercolani E, Duplat J and Gully P 2017 *Appl. Therm. Eng.* **126** 1023
[9] Jun S and Kim SJ 2019 *Int. J. Heat Mass Transfer* **134** 321
[10] Nikolayev VS 2013 *Int. J. Heat Mass Transfer* **64** 313
[11] Aussillous P and Quéré D 2000 *Phys. Fluids* **12** 2367
[12] Zhang X and Nikolayev VS 2021 *Proc. Joint 20th IHPC and 14th IHPS* (Gelendzhik, Russia)
[13] Bae J, Lee SY and Kim SJ 2017 *Energy Convers. Manage.* **151** 296
[14] Nikolayev VS 2011 *Int. J. Heat Mass Transfer* **54** 2226
[15] Gully P, Bonnet F, Nikolayev VS, Luchier N and Tran TQ 2014 *Heat Pipe Sci. Technol.* **5** 369
[16] Nikolayev V and Marengo M 2018 Pulsating heat pipes: Basics of functioning and numerical modeling *Encyclopedia of Two-Phase Heat Transfer and Flow IV*, vol. 1: Modeling of Two-Phase Flows and Heat Transfer, JR Thome, ed. (World Scientific) pp. 63 – 139
[17] Tessier-Poirier A, Monin T, Léveillé E, Monfray S, Formosa F and Fréchette LG 2019 *Phys. Rev. Fluids* **4** 103901
[18] Rao M 2015 *Thermo-hydrodynamics of an extended meniscus as unit-cell approach of pulsating heat pipe* Ph.D. thesis Institut National des Sciences Appliquées de Lyon URL https://tel.archives-ouvertes.fr/tel-01247470
[19] Schlichting H 1968 *Boundary-Layer Theory* (Ney York: McGraw-Hill)